

1 **The effects of Hurricane Harvey on Texas coastal zone chemistry**

2 Piers Chapman^{1,2}, Steven F. DiMarco^{1,2}, Anthony H. Knap^{1,2}, Antonietta Quigg^{1,3}, Nan D.
3 Walker⁴

4

5 1. Department of Oceanography, Texas A&M University, College Station, TX 77843
6 2. Geochemical and Environmental Research Group, Texas A&M University, College
7 Station, TX 77843
8 3. Department of Marine Biology, Texas A&M University, Galveston, TX 77553
9 4. Department of Oceanography and Coastal Sciences, Louisiana State University, Baton Rouge,
10 LA, 70803

11

12 *Correspondence to:* Piers Chapman (piers.chapman@tamu.edu)

13

14 **Abstract**

15 Hurricane Harvey deposited over 90 billion cubic meters of rainwater over central Texas, USA,
16 during late August/early September 2017. During four cruises (June, August, September and
17 November 2017) we observed changes in hydrography, nutrient and oxygen concentrations in
18 Texas coastal waters. Despite intense terrestrial runoff, nutrient supply to the coastal ocean was
19 transient, with little phytoplankton growth observed and no hypoxia. Observations suggest this
20 was probably related to the retention of nutrients in the coastal bays, rapid uptake by
21 phytoplankton of nutrients washed out of the bays, as well as dilution by the sheer volume of
22 rainwater, and the lack of significant carbon reserves in the sediments, despite the imposition of
23 a strong pycnocline. By the November cruise conditions had apparently returned to normal and
24 no long-term effects were observed.

25

26

27 **Keywords**

28 Hurricane Harvey, Texas coast, nutrients, oxygen, chlorophyll

30 **1. Introduction**

31 The Gulf of Mexico is renowned for its hurricanes and tropical storms, and 2017 was a very
32 active year in the Atlantic, with 10 hurricanes and 8 tropical cyclones and depressions. Hurricane
33 Harvey developed in the Bay of Campeche, in the extreme southwest of the Gulf of Mexico, on
34 23 August, 2017, intensifying rapidly on **24 August** over water with SST >30° C and an upper
35 ocean heat content anomaly (measured by three ARGOS floats) that extended to ~45 m water
36 depth (Trenberth et al., 2018). Harvey crossed the edge of the Texas shelf in the northwestern
37 Gulf at 18.00 U.S. Central Time having intensified to category 3, and reached category 4
38 strength by midnight of **25 August** with sustained wind speeds of 60 m s⁻¹ (115 kt) and a
39 minimum central pressure of 937 mbar (Blake and Zelinsky 2018). Rapid intensification of
40 tropical cyclones over the shallow waters of the south Texas shelf has been reported previously
41 and is believed to be related to periods when warm water occupies the whole water column. This
42 prevents mixing of colder bottom water that can reduce the energy flux feeding the hurricane
43 (Potter et al., 2019). The storm came ashore near Corpus Christi, TX on 26 August, and stalled
44 over the TX coast, moving slowly to the northeast until August 31, after which it moved inland
45 and dissipated over Kentucky (Fig. 1).

46
47 Harvey brought a storm surge of up to 3 m and widespread torrential rain to the Texas coast,
48 with the heaviest rainfall, over 1500 mm (60 in), measured at Nederland and Groves, near
49 Houston (Blake and Zelinsky, 2018). Heavy rain (<500 mm) also affected Louisiana (Fig.1).
50 This unprecedented rainfall, the highest ever recorded in the U.S. for a tropical cyclone, resulted
51 in widespread flooding in **Texas and Louisiana** (Emanuel, 2017; Balaguru et al., 2018). It is
52 estimated that the total volume of rainfall over Texas and Louisiana during Harvey's passage
53 was between $92.7 \times 10^9 \text{ m}^3$ (Fritz and Samenow, 2017), and $133 \times 10^9 \text{ m}^3$ (DiMarco,
54 unpublished), and over 200 mm of rain was recorded as far inland as Tennessee and Kentucky as
55 the storm died down (Blake and Zelinsky, 2018; Fig.1). In addition to the rain that fell on land,
56 DiMarco (unpublished) has estimated that about another $44 \times 10^9 \text{ m}^3$ fell over the ocean.

57

Commented [PC1]: Deleted sentence on damage

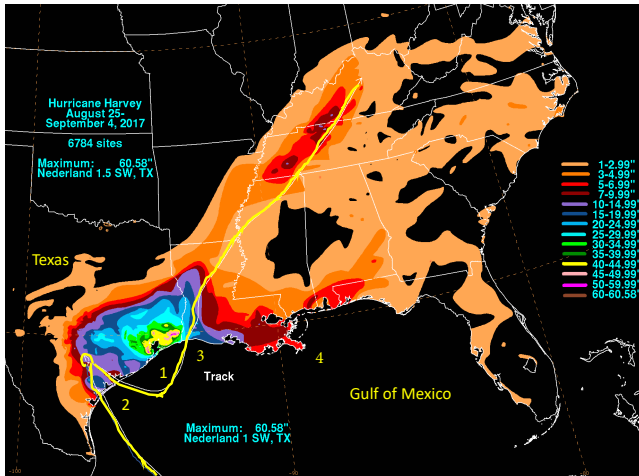


Fig 1

58

59

60 Fig. 1. Track of Hurricane Harvey and associated rainfall (in inches) over the southern United States, 24 August-4
 61 September, 2017 (from Blake and Zelinsky, 2018). The numbers 1, 2 and 3 denote the positions of Galveston Bay,
 62 Matagorda Bay, and Lake Sabine respectively. The Mississippi delta (in Louisiana) is shown as 4. The Nederland
 63 1.5 SW rain gauge, which recorded the highest rainfall, is at 29.95°N, 94.01°W.

64

65 Galveston Bay collects the runoff from the Houston metropolitan region. Following the storm,
 66 the bay became a freshwater lake (Du et al., 2019; Steichen et al., 2020; Thyng et al., 2020) as it
 67 was flushed with about three to five times its volume of rainwater. U.S. Geological Survey
 68 (USGS) data (downloaded from <https://waterdata.usgs.gov> on 25 June 2020; all such records are
 69 collected in cubic feet per second (cfs) and have been converted to $m^3 s^{-1}$) show very rapid
 70 increases in flow rates in Texas rivers and streams following the storm's landfall. For instance,
 71 flows in the Colorado and Brazos Rivers south of Galveston Bay (USGS stations 08162000 and
 72 08111500 respectively; Figs S1a and S1b) increased from <2,000 cfs ($\sim 60 m^3 s^{-1}$) during most of
 73 August to over 90,000 cfs ($> 2,500 m^3 s^{-1}$) by the beginning of September, while flow in the San
 74 Jacinto River (USGS station 08068090, Fig. S1c) and the Trinity River at Liberty (USGS station
 75 08067000, Fig. S1d), which both flow into Galveston Bay, exceeded 100,000 cfs ($3,400 m^3 s^{-1}$).
 76 The gauge at Liberty was unfortunately not operational immediately prior to 27 August or after 9
 77 September, but during June flowrates were typically 10,000 – 14,000 cfs ($\sim 300-420 m^3 s^{-1}$). Such

78 large changes in runoff are known to produce major changes in estuaries and coastal waters (e.g.,
79 Ahn et al., 2005; Paerl et al., 2001, 2006; Mallin and Corbett, 2006; De Carlo et al., 2007; Zhang
80 et al., 2009; Du et al., 2019; Thyng et al., 2020). Liu et al. (2019) and Steichen et al. (2020)
81 reported changes in the phytoplankton community within Galveston Bay as the salinity
82 decreased and then increased again.

83

84 The massive runoff led to turbidity plumes visible well offshore (Fig. S2). D'Sa et al. (2018)
85 monitored large increases in terrestrial carbon (25.22×10^6 kg) and suspended sediments (314.7
86 $\times 10^6$ kg) entering Galveston Bay during the period 26 August-4 September. The plume off
87 Galveston Bay on 31 August extended at least 55 km offshore (Du et al., 2019), and surface
88 water with a salinity of 15 was measured on 1 September at the Texas Automated Buoy System
89 (TABS) buoy F (28.84°N , 94.24°W ; yellow diamond in Fig. S2), where it is typically 31-32
90 (data from <https://tabs.gerg.tamu.edu>, downloaded on 6 June 2018). Normal salinities did not
91 return until 8 September. Similar sediment plumes at the mouths of the Brazos and Guadalupe
92 estuaries can be seen in Fig. S2, and such plumes and lowered salinities have been reported from
93 the Lavaca-Colorado and Nueces-Corpus estuaries near Corpus Christi (Walker et al., 2021). It is
94 likely that other bays and estuaries along the Texas coast were similarly affected, as they were all
95 under the path of the hurricane.

96

97 We report here on data collected before and after the hurricane along the Texas coast between
98 Galveston and Padre Island, south of Corpus Christi, Texas. Two cruises were completed prior to
99 the hurricane as part of a separate project. Following the hurricane, we completed three more
100 cruises, occupying the same stations in September (twice) and November 2017. This paper
101 reports on the changes in the water column between the pre- and post-hurricane cruises as they
102 relate to stratification, nutrient supply and oxygen concentrations.

103

104 2. Methods

105 Pre-hurricane cruises on the R.V. *Manta* took place from 12-16 June and 7-11 August 2017,
106 while post-hurricane cruises were from 22-27 September, 29 September – 1 October, and 15-20
107 November on the R.V. *Point Sur*. The 27 September-1 October cruise only occupied the two
108 inshore stations on each line; all other cruises covered a standard grid of five lines of five

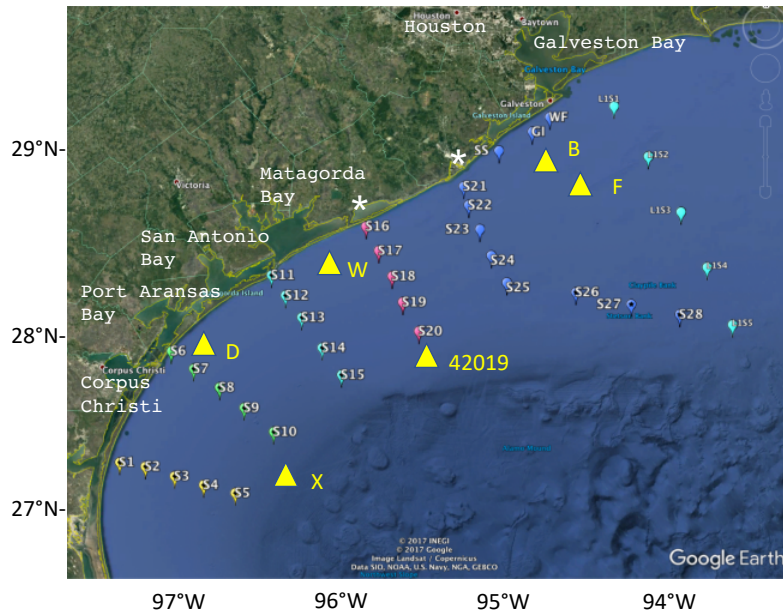
109 stations each (Fig. 2), together with supplemental *ad hoc* stations between lines and offshore in
110 the east of the region towards the Flower Gardens Banks National Marine Sanctuary, a shallow
111 reef system 120 km south of Galveston Bay near 27.92°N, 93.75°W. During the November
112 cruise, stations were added at the outer ends of the southernmost lines to ensure sampling of
113 offshore surface water with salinity >35. Depths at the outer ends of each line decreased from
114 95-110 m at stations 5 and 10 to 85 m at station 15, and 50 m at stations 20 and 25.

Commented [PC2]: Deleted "additional"

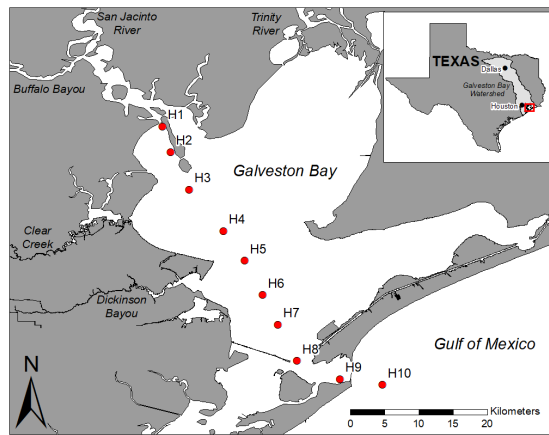
115
116 At each station, a full-depth CTD cast was made using a SeaBird 911 CTD fitted with a SBE-55
117 temperature sensor, SBE-3 conductivity sensor, SBE-45 pressure sensor, and a SBE-43 oxygen
118 probe. Additional sensors on the rosette package included a Chelsea Instruments Aqua3
119 fluorometer and a Biospherical/Licor PAR sensor. Discrete samples were collected from a 6-bottle
120 rosette for salinity determinations ashore (+/- 0.002) and for oxygen calibration (+/- 0.3 μ mol/L),
121 by Winkler titration on board ship. Nutrient samples were collected, filtered, frozen on board and
122 analyzed ashore for nitrate, nitrite, phosphate, silicate, and ammonia by standard autoanalyzer
123 methods (WHPO 1994). Limits of detection (and precision) are about 0.1 μ mol/L for nitrate
124 (2%), silicate (1%) and ammonia (3%), and 0.02 μ mol/L for nitrite (1%) and phosphate (2%).
125 Local meteorological data were collected by the ship's system, while surface water temperature
126 and salinity data came from the ships' flow-through system.

127
128 Wind and current data are available from the TABS moorings along the Texas coast (see Fig. 2
129 for positions and <http://tabs.gerg.tamu.edu> for the data archive). Buoy B (off Galveston)
130 provided both wind and current data from before Harvey's landfall with a gap in the first half of
131 August; buoys W (off Matagorda Bay) and D (off Corpus Christi) provided current data only.
132 We have used additional wind data from TABS buoy X, which provided data until it failed on
133 the morning of 25 September, and NOAA buoy 42019 (29.91°N, 95.34°W, obtained from the
134 National Data Buoy Center at <https://www.ndbc.noaa.gov>, downloaded 7 July 2020).

135
136 Fluorometer data were obtained at each station sampled using a Chelsea Aqua 3 instrument on
137 the rosette. This instrument was calibrated prior to and after the cruises, but not immediately.
138 Satellite imagery (Aqua-1 MODIS sensor, Level 2 Ocean Color files) downloaded from the
139 NASA Goddard ocean color website (<https://oceancolor.gsfc.nasa.gov>, downloaded 25 May



140



141

142 Fig. 2. Stations occupied during the four cruises. Only stations S1-S25 and the inshore stations GI, SS and WF were
143 occupied during June and August. All stations shown were occupied in the 22-27 September cruise and in
144 November. Only the two inshore stations on each line were occupied during the second September cruise. Yellow
145 triangles show positions of TABS moorings B, D, F, W and X, and NOAA buoy 42019. White stars show the
146 mouths of the Colorado River (near station 16) and Brazos River (near station 21). Data from stations 11-15 are
147 shown in Figs. 5, 6 and supplementary figures. (b) Galveston Bay and vicinity showing Trinity and San Jacinto
148 rivers and stations discussed in Fig. 8.

149

150 2019) were processed using the NASA SeaDAS software. In reality, the satellite-derived values
151 may be too high, due to the presence of CDOM after the storm (D'Sa et al., 2018), as the OC3
152 algorithm provided by the SeaDAS software cannot discriminate between chlorophyll *a* and
153 CDOM.

154

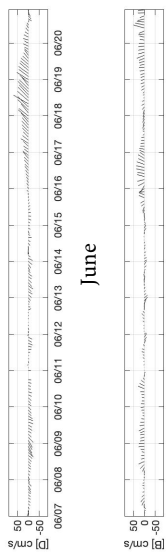
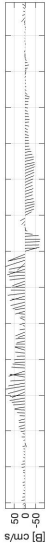
155 3. Results

156 3.1 Wind fields

157 Wind data from all moorings (not shown) were typical of summer conditions in this part of the
158 Gulf of Mexico, being predominantly from the south with occasional reversals (Nowlin et al.,
159 1998). At TABS buoy B, wind velocities during June and July were generally 5-8 m s^{-1} and
160 varied between SSE and SSW. Following a gap in data from 31 July until 22 August, they
161 remained in this quadrant until the passage of the hurricane, although wind speeds increased
162 from 3-4 m s^{-1} on 22 August to 12 m s^{-1} on 29 August when they were from the north. After the
163 hurricane, September winds again were predominantly from the SE/SSE, with the exception of
164 two short-lived reversals on 5 and 10-12 September, with wind speeds around 4-7 m s^{-1} .

165

166 Further south and offshore, at TABS mooring X and NOAA mooring 42019, weak northerly
167 winds (generally <4 m s^{-1}) occurred from 6-8 June, with a second northerly spell from 20-22
168 June, when speeds reached 10 m s^{-1} at mooring X and 15 m s^{-1} at 42019. After this second frontal
169 system, winds reverted to SE/SSE at both moorings until the passage of Hurricane Harvey at the
170 end of August. During September, at mooring 42019, winds were primarily from the NNE/ENE
171 at 4-10 m s^{-1} until the 12th, and again from the 27th, with SE or easterly winds of 3-7 m s^{-1} from
172 14-26 September. Maximum sustained wind speeds recorded during the hurricane at this
173 mooring were 17 m s^{-1} , with gusts to 22.6 m s^{-1} . During October, there were two northerly/



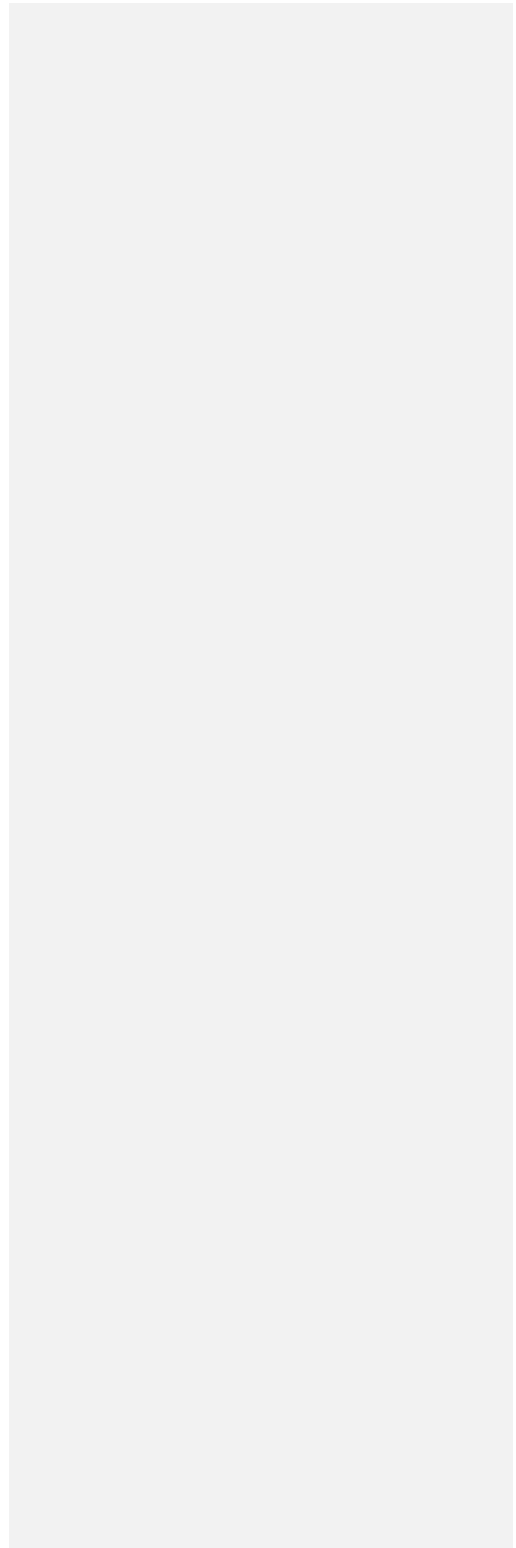
June

August



September

November



175 Fig. 3. Current vectors at TABS buoys B, D and W during the cruise in June, the period of the hurricane (August),
176 and the cruises in September and November.

177
178 westerly wind events, on the 16th, when winds reached speeds of 15 m s^{-1} , and a sustained event
179 from 25-28 October, again with speeds $<15 \text{ m s}^{-1}$. Northerly winds continued during November,
180 with sustained winds of 12-14 m s^{-1} during the periods 8-11, 18-20, and 22-24.

181
182 **3.1 Water movement**

183 Water movement over the Texas shelf is typically downcoast (towards the southwest) in non-
184 summer months and upcoast (towards the northeast) in summer, with currents following the wind
185 (Cochrane and Kelly, 1986; Walker, 2005). Upcoast winds and currents promote upwelling and
186 act to retain water from the Mississippi-Atchafalaya system on the east Texas-Louisiana shelf
187 (Hetland and DiMarco, 2008), while downcoast flow is downwelling-favorable and can reduce
188 local stratification. During June 2017, currents at Buoy D (27.96° N, 96.84° W) were essentially
189 downcoast from prior to the cruise until 15 June, when they switched to upcoast until 20 June,
190 after which they flowed downcoast again (Fig. 3a). The current reversal took place slightly later
191 (17 June) at Buoys B (28.98° N, 94.90° W) and W (28.35° N, 96.02° W), but the return to
192 downcoast flow again occurred on 20 June at both sites (Fig. 3a). These three moorings are all
193 situated close to the coast in water depths of 20 +/- 2 m.

194
195 Upcoast currents prevailed at sites W and D during the August cruise (Fig. 3), although currents
196 were downcoast from about 8-10 August at W and 9-11 August at site D (not shown). Buoy B
197 did not record current speeds during this period, but was back in service immediately before the
198 hurricane arrived. During the passage of the hurricane, the southernmost mooring (buoy D)
199 recorded strong currents of $> 1 \text{ m/s}$ which changed from downcoast to upcoast and back to
200 downcoast again as the storm moved towards the northeast (Fig. 3b). Buoy W recorded
201 continuous downcoast currents during the period of the hurricane, while buoy B showed strong
202 onshore currents ($<1.0 \text{ m s}^{-1}$) until 30 August, when currents reversed to offshore at $< 80 \text{ cm s}^{-1}$.
203 Following the hurricane, coastal currents were considerably weaker at all three sites in
204 September and November. During the September cruise there were a number of current
205 reversals, especially at buoy W, although velocities were generally $<30 \text{ cm s}^{-1}$ (Fig. 3c). By

206 November, current velocities decreased still further and the expected flow towards the west was
207 reinstated (Fig. 3d).

208

209 **3.2 Temperature, precipitation and salinity**

210 Temperatures (not shown) showed well-mixed or weakly stratified water inshore in June and
211 August with surface-bottom differences of less than 2°C at the two inshore stations on each line.
212 Further offshore, bottom temperatures decreased with depth but there remained a well-mixed
213 surface layer of 15-25m thickness. Following the hurricane, however, the mixed layer extended
214 offshore to the third station on each line in September and almost all stations in November, when
215 isothermal water was found as deep as 80m in some instances, and bottom temperatures were
216 often warmer than at the surface.

217

218 Surface temperatures increased from about 28.5 °C in June to over 30 °C in August (Trenberth et
219 al., 2018). As the hurricane passed, temperatures at the buoys, including at NBDC buoy 42019
220 (27.91° N, 95.34° W), decreased to a minimum of about 27.5 °C, but recovered to 28.5-29 °C by
221 the September cruises. By November, temperatures had decreased to 21-22 °C, 22-23 °C and 23-
222 23.5 °C at buoys B, W and D respectively. NBDC buoy 42019, which is further offshore in 82 m
223 of water, registered temperatures between 25.4° and 26.0°C during this period.

224

225 Precipitation **measurements** for a number of stations in central Texas is shown in Table 1. With
226 the exception of the August data, all stations reported lower than average rainfall during these
227 months apart from Houston Intercontinental Airport in June and July, and Austin International
228 Airport in September (respectively north and northwest of Galveston Bay). Despite this, low
229 salinities were found in June at the surface inshore and pushing southwards (Fig. 4a), with a
230 strong, sloping salinity front between the surface layer and the deeper water. Salinity values
231 across the front changed by **~12** along stations 18-20 and 21-23 just south of Galveston Bay. The
232 salinity gradient decreased towards the south, with an inshore-offshore change of only **4** south of
233 28°N. The lowest surface salinity (station 21) was <22 at this time, and was still <32 along the
234 southernmost line except at the outermost station. Bottom water salinities (not shown) were
235 higher because of density stratification, with salinities of >35 found in water deeper than about
236 20m at stations in the eastern half of the grid and 35 m on the southern lines. The low surface

Commented [PC3]: Deleted "psu"

Commented [PC4]: Deleted "psu"

237

238 Table 1. Precipitation (cm) for sites in central Texas from May-September 2017 compared with the long-term mean
239 (italics). Data downloaded from https://www.srcc.tamu.edu/climate_data_portal/?product=precip_summary
240 (accessed 7.07.2021).

241

	May	June	July	Aug	Sept
Austin International airport (30.20°N, 97.66°W)	7.59 <i>11.86</i>	6.17 8.28	2.69 <i>4.65</i>	32.99 6.20	9.68 <i>8.46</i>
Corpus Christi airport (27.77°N, 97.50°W)	8.18 <i>8.51</i>	4.90 8.00	3.22 <i>5.97</i>	14.98 7.87	3.71 <i>13.41</i>
Houston Hobby airport (29.65°N, 95.28°W)	6.81 <i>12.80</i>	13.20 <i>13.84</i>	7.92 <i>11.40</i>	98.73 11.81	9.52 <i>13.13</i>
Houston Intercontinental airport (29.99°N, 95.34°W)	6.12 <i>13.59</i>	18.26 14.22	15.98 <i>9.45</i>	99.34 11.10	3.12 <i>12.09</i>
San Antonio airport (29.53°N, 98.46°W)	4.48 <i>10.18</i>	1.02 8.58	0.41 5.92	14.91 6.12	7.11 9.32
Victoria airport (28.84°N, 96.92W)	7.77 <i>12.85</i>	8.92 11.10	0.94 8.25	43.03 7.82	7.92 <i>12.52</i>

260

261 salinities resulted from westward flow from the Mississippi-Atchafalaya river system (MARS),
262 together with local outflow from Galveston Bay. MARS peak flow during the 2017 spring flood
263 was $34,500 \text{ m}^3 \text{ s}^{-1}$, almost double the long-term mean from 1935-2017 (data from
264 <http://rivergages.mvr.usace.army.mil/>, accessed 7 July 2021).

265

266 By August (Fig.4b), surface salinities had increased across the region as a result of the southerly
267 winds, with a minimum of 32.15 just south of Galveston Bay, while the 35 surface isohaline was
268 situated off Matagorda Bay between stations 16-20 and 11-15. Bottom water was still stratified
269 at stations on the two northern lines, with salinities <35 only found at stations 16, 17, 21 and 22
270 and at the Wind Farm (29.14°N, 94.75°W). Further south, stations 1-10 and 13-15 all contained
271 almost isohaline water with S>36.

272

273 The fresh water from the hurricane caused a major change in the surface salinity by the time of
274 the first September cruise (22-27), resulting once again in a strong cross-shelf gradient (Fig. 4c).

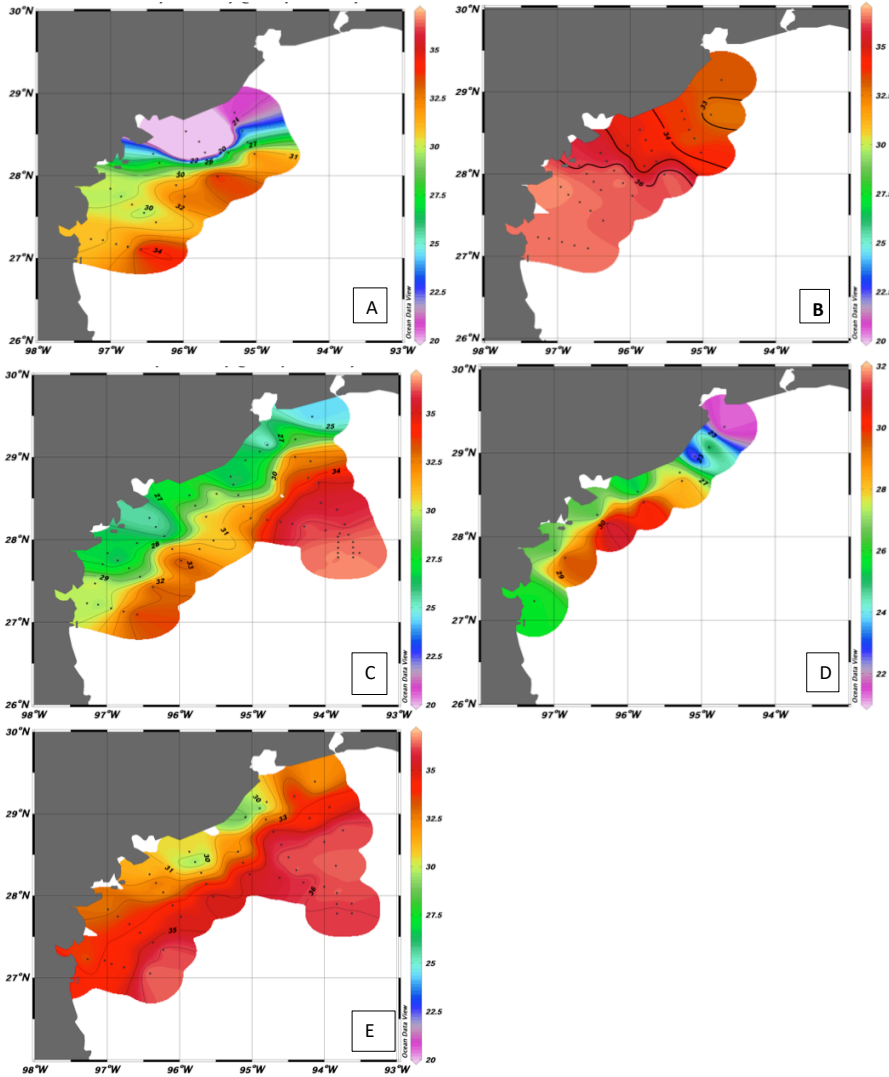


Fig. 4. Surface salinities during 2017 cruises in (a) June, (b) August, (c) 22-27 September, (d) 29 September – 1 October, and (e) November.

275

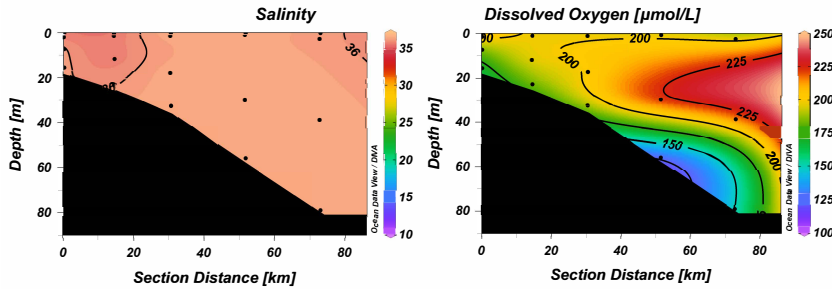
276

277 Surface salinities were <33 throughout the region, apart from two stations at the extreme south of
278 the grid, and in the area more than 100 km offshore between Galveston Bay and the Flower
279 Gardens Banks, where there was a strong salinity front. A similar situation was found a week
280 later at the inshore stations (Fig. 4d), although the surface layer of low salinity water had thinned
281 and was confined to the innermost stations on each line. Vertical sections in September showed
282 very strong stratification of up to 10 **in salinity** within a 10-m depth interval along all lines (e.g.,
283 Fig. 5; this section across stations 11-15, adjacent to Matagorda Bay, is taken as representative
284 for all five lines). The halocline was not flat, but deepened towards the coast, giving a wedge of
285 lower salinity water onshore, and the depth at which it intersected the bottom decreased from
286 ~30m in the north to less than 20m in the south. Water with salinity > 36 was found at the
287 bottom on all lines. By November (Figs 4e, 5), however, a more typical salinity field was found,
288 with well-mixed water throughout the coastal zone and a general onshore-offshore gradient at all
289 depths. This is normal for the region in the fall, when atmospheric frontal systems tend to move
290 across the Texas shelf and break down the summer pycnocline (Cochrane and Kelly, 1986;
291 Nowlin et al., 1998).

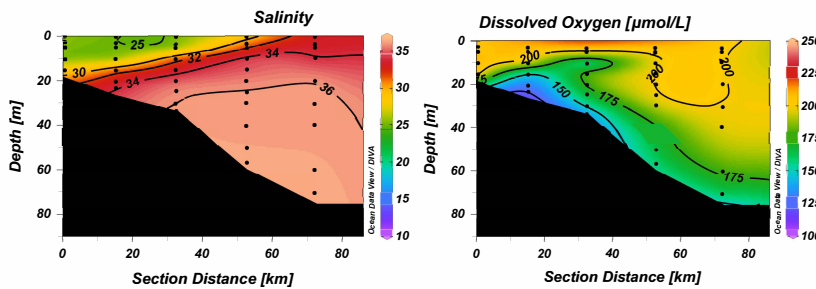
292

293 **3.3 Oxygen concentrations**

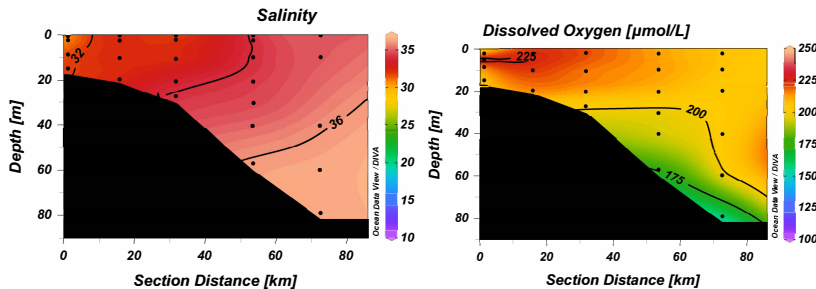
294 Oxygen concentrations in this region of the Gulf of Mexico are typically saturated above the
295 pycnocline, as found during all four cruises. Concentrations varied between 210-220 $\mu\text{mol/L}$ in
296 June (not shown), when the SST was about 25° C, and 190-215 $\mu\text{mol/L}$ during August and
297 September, when it was nearer 30° C (Fig. 5). **Oxygen saturation in seawater of salinity 35 is 206**
298 **$\mu\text{mol/L}$ at 25°C and 190 at 30°C**. By November, with declining surface temperatures, the
299 saturation concentration increased to between 210-230 $\mu\text{mol/L}$. Below the pycnocline, oxygen
300 concentrations declined in the higher salinity water. This effect was most pronounced offshore in
301 June and August, when subtropical underwater, with typical oxygen concentrations of 160-170
302 $\mu\text{mol/L}$, intruded onto the outer shelf (Fig. 5). Isolated patches with concentrations <150 $\mu\text{mol/L}$
303 were seen over the mid-shelf and across the eastern part of the grid at this time. By September,
304 bottom concentrations of 150 $\mu\text{mol/L}$ or less were found over large parts of the inner and middle
305 shelf and at the outermost stations of the grid. Vertical sections showed lowest oxygen
306 concentrations at the base of the pycnocline where it intersected the seafloor (Fig. 5), but
307



A



B



C

308
309 Fig. 5. Salinity (psu) and oxygen ($\mu\text{mol/L}$) sections across line 3 (stations 11-15) for the August (a), first September
310 (b) and November (c) cruises.

311

312 hypoxia (oxygen concentrations $<62 \mu\text{mol/L}$) was not observed at any station. There was little
313 change in either the pattern of oxygen distribution or concentrations at the innermost stations

314 between the two cruises in September (not shown). By November, however, after the passage of
315 a number of frontal systems with wind speeds up to 14 m/s, the oxygen concentrations showed
316 little vertical structure and the system could be said to have returned to normal for that month.

317

318 **3.4 Nutrients**

319 Nutrient concentrations in the coastal waters and bays along the Texas coast in summer are
320 typically very low at the surface, increasing with depth even on the shallow shelf as nutrient
321 regeneration takes place near the bottom. This is especially the case when hypoxic events occur
322 (Nowlin et al., 1998; DiMarco and Zimmerle, 2017; Bianchi et al., 2010). Mean concentrations
323 in the upper 30m of the water column for all nutrients at stations within the grid as well as at
324 additional stations having water depths shallower than 50m are given in Table 2. Data from the
325 second September cruise, which covered only the two inshore stations on each line, are not
326 included in the table. These data showed similar patterns to the cruise a week earlier, although
327 mean concentrations were higher because of the proximity of the coast and the many freshwater
328 discharges from bays and rivers.

329

330 In higher salinity (>35) water and offshore, nutrient concentrations increase only slowly with
331 depth and nitrate and silicate concentrations $> 5 \mu\text{mol/L}$ are generally found in midwater only
332 below depths of about 50 and 100m respectively (Fig. 6, Supplemental Fig. S3). Only one nitrate
333 sample (in September) containing more than $8 \mu\text{mol/L}$ came from below 60m depth. Nitrite
334 concentrations were almost all low, with mean concentrations in the upper 30m below 0.5
335 $\mu\text{mol/L}$ on all four cruises, although individual surface concentrations were considerably higher.

336

337 Ammonia concentrations were variable, particularly inshore, but generally provided a
338 background concentration of about $2-4 \mu\text{mol/L}$. As a result, DIN distribution resembled that for
339 nitrate but with the added background contribution from ammonia (Fig. S4). Phosphate
340 concentrations (not shown) were similarly lower at the surface than at depth, except in
341 September, when surface runoff increased concentrations above $3 \mu\text{mol/L}$ in the upper 10m of
342 the water column and to a background concentration between $1.5 - 3 \mu\text{mol/L}$ in the rest of the
343 water column up to 50 km offshore (between stations 13 and 14). Phosphate is almost always
344 non-limiting for phytoplankton in this region, so that residual phosphate concentrations can be

345

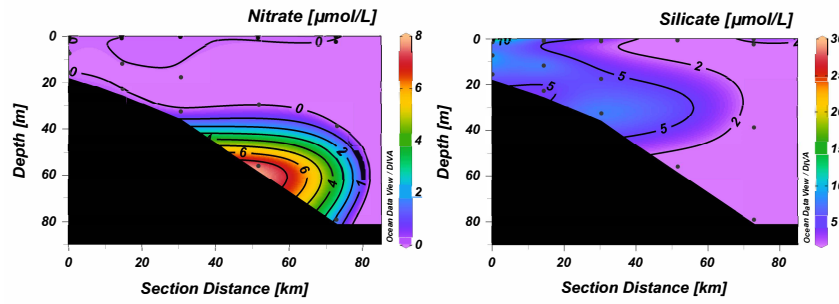
346 Table 2. Mean and range ($\mu\text{mol/L}$) and number of samples (N) for nitrate, nitrite, ammonia, phosphate and silicate in

347 the upper 30m of the water column for all four cruises. DIN is calculated as the sum of the three nitrogen species.

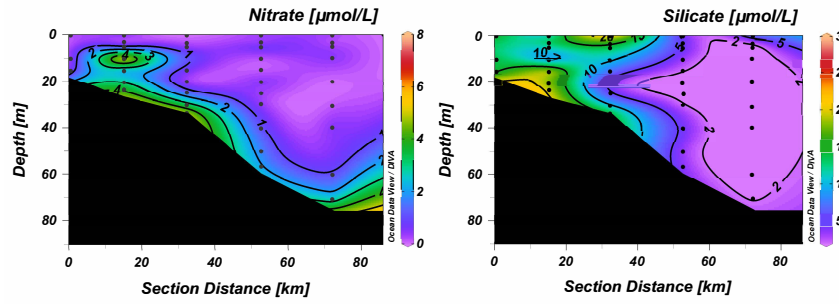
348 DIN:P and DIN:Si ratios use the values for all individual samples.

349

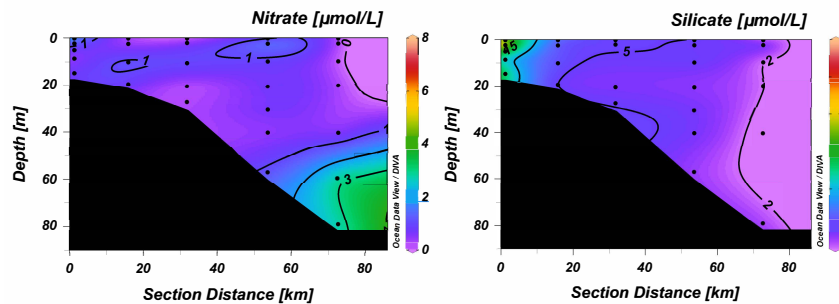
		June	August	September	November
Nitrate	Mean	0.71	0.10	0.57	0.52
	Range	0.00-10.60	0.00-1.98	0.00-7.41	0.00-1.98
	N	85	94	194	164
Nitrite	Mean	0.43	0.18	0.44	0.36
	Range	0.00-2.80	0.00-1.04	0.03-4.76	0.00-1.13
	N	86	98	196	172
Phosphate	Mean	1.07	0.65	1.30	1.00
	Range	0.21-2.85	0.00-3.55	0.00-5.63	0.00-3.24
	N	85	91	190	169
Silicate	Mean	6.00	5.04	7.00	7.76
	Range	1.18-26.89	0.00-20.09	0.00-40.23	0.94-25.71
	N	84	89	193	168
Ammonia	Mean	1.90	3.74	2.39	2.91
	Range	0.00-7.62	1.37-8.05	0.08-4.97	0.89-4.80
	N	84	87	192	162
DIN	Mean	3.01	3.70	3.37	3.72
	Range	0.01-14.47	0.14-8.56	1.02-12.35	1.05-7.03
	N	85	95	191	160
DIN:P		3.56	11.95	4.98	10.11
	Range	0.03-25.86	0.00-324	0.00-138	0.00-381
		0.63	2.59	1.17	0.78
DIN:Si	Range	0.00-3.20	0.00-53.29	0.00-25.21	0.10-4.78



A



B



C

350
351 Fig. 6. Nitrate and silicate ($\mu\text{mol/L}$) sections along line 3 (stations 11-15) during August (a), first September (b) and
352 November (c) cruises.

353 found even though nitrate is depleted (Bianchi et al., 2010), although Sylvan et al. (2006, 2007)
354 and Quigg et al. (2011) have suggested phosphate limitation can occur further east in the
355 Mississippi plume. Silicate, however, showed an opposite trend to the general pattern of the
356 other elements, with almost all samples $>15 \mu\text{mol/L}$ coming from the upper 25m of the water
357 column, and concentrations decreased with depth to $<5 \mu\text{mol/L}$ below 100m (Figs 6, S3). Silicate
358 also showed a cross-shelf gradient, particularly along the two southernmost lines (not shown).

359

360 This general distribution shown in Figs. 5 and 6 was seen during early summer along all the lines
361 occupied during June and August. In June, high concentrations of both nitrate and silicate were
362 seen at stations 21 and 22, immediately south of Galveston Bay, where bottom water oxygen
363 concentrations were $<90 \mu\text{mol/L}$; elsewhere midwater levels of both elements were low, with
364 very low nitrate concentrations ($<0.5 \mu\text{mol/L}$) being found even at the bottom at some stations.
365 While silicate concentrations were more variable, highest concentrations were typically again
366 seen at the bottom, and midwater concentrations were generally $<5 \mu\text{mol/L}$. The situation was
367 similar in August (Fig. 6), when nitrate was very low throughout the region, and even bottom
368 nitrate values were below detection at many stations.

369

370 In September, despite the extreme freshwater runoff, nitrate concentrations were still low except
371 near the bottom at shallow stations, and there was little sign of any surface or mid-water increase
372 in concentration (Fig. 6). A comparison of nitrate concentration with depth gave essentially the
373 same distribution as during earlier cruises, although there were more samples above $2 \mu\text{mol/L}$
374 within the 10-30m depth range (Fig. S3). These were bottom samples at shallow stations with
375 lower oxygen concentrations. The cross-shelf gradient in silicate concentrations was more
376 pronounced on this cruise, and concentrations were $>10 \mu\text{mol/L}$ throughout the water column at
377 all the inshore stations. However, by November, concentrations of both nutrients had decreased
378 considerably, although the offshore silicate gradient was still present and concentrations >10
379 $\mu\text{mol/L}$ were found inshore (Fig. 6). Phosphate concentrations higher than $2 \mu\text{mol/L}$ were seen
380 only in September (Table 2), suggesting, along with the increased silicate, the presence of
381 terrestrial runoff following the hurricane.

382

383 Oxygen/nitrate and oxygen/silicate covariance plots are shown in Supplemental Fig. S5. High
384 nitrate values at oxygen concentrations greater than 200 $\mu\text{mol/L}$ in August and September (22-
385 27) are from samples taken in low salinity surface water; where oxygen concentrations were
386 below 150 $\mu\text{mol/L}$ the increase in nitrate concentration is caused either by regeneration over the
387 shelf or by the intrusion of deeper Subtropical Underwater. During these two cruises, higher
388 nitrate and silicate concentrations were associated generally with lower oxygen concentrations
389 (Fig. S5), although some surface samples on both cruises showed relatively high values,
390 associated with salinities < 35.

391

392 Quigg et al. (2011) state that DIN concentrations <1 $\mu\text{mol/L}$ and a DIN:P ratio <10 indicate
393 nitrogen limitation, with P <0.2 $\mu\text{mol/L}$ and DIN:P >30 indicating P limitation and Si <2
394 $\mu\text{mol/L}$, DIN:Si >1 and Si:P <3 showing Si limitation. As shown in Table 2, DIN:P and DIN:Si
395 ratios for individual samples in the upper 30m of the water column were low during all four
396 cruises, with mean DIN:P being less than the 16:1 Redfield ratio throughout, while the mean
397 DIN:Si ratio was >1 only in the August and September cruises. This suggests both nitrogen
398 limitation throughout the period and possible silicate limitation of diatom growth during August
399 and September despite the background levels of ammonia that contributed to the DIN
400 concentration. While individual samples had higher ratios, these all occurred when either
401 phosphate or silicate concentrations were measurable but very low in comparison with DIN
402 concentrations (<0.1 $\mu\text{mol/L}$ for P and <0.5 $\mu\text{mol/L}$ for Si). The ratios of the mean
403 concentrations of DIN across the region to the mean concentrations of P and Si (e.g., 3.01:1.07
404 for DIN:P in June), were 2.81 and 0.50, 5.69 and 0.73, 2.59 and 0.48, and 3.72 and 0.48 for the
405 June, August, September and November cruises respectively, again suggesting nitrogen
406 limitation.

407

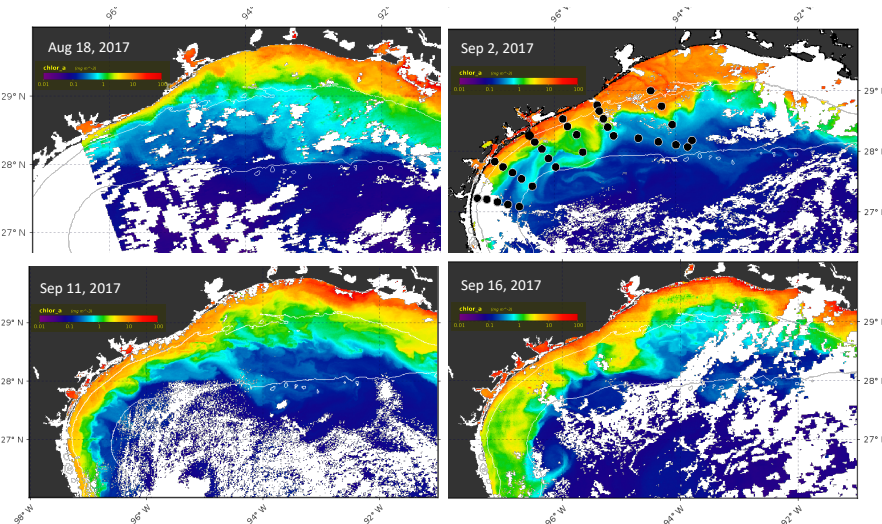
408 **3.5 Chlorophyll**

409 Chlorophyll concentrations were examined using both in situ fluorescence data obtained during
410 the cruises and satellite imagery from the MODIS sensor on the Aqua satellite (Fig. 7). The
411 Texas coast and northwestern Gulf of Mexico were covered with clouds during the pre-Harvey
412 and post-Harvey cruises, however a time-history of four high quality chlorophyll-*a* images on 18

Commented [PC5]: New section, moved from Discussion in previous version

413 August (pre-Harvey), 2 September (6 days post-Harvey), 11 September and 16 September 2017
414 revealed shelf events between the two cruises closest to Harvey's landfall.

415
416 Fluorescence data (not shown) from the CTD casts taken during all cruises were almost
417 invariably $<1 \text{ mg m}^{-3}$, especially in the upper mixed layer, suggesting little productivity
418 immediately before or during the cruises. During the 22-27 September cruise only 4 of 37



419
420 Fig. 7. Aqua-1 MODIS imagery depicting chlorophyll α estimates for 18 August, 2 September, 11 September and 16
421 September, 2017. White areas along the Louisiana shelf and offshore are clouds. Thin white lines denote 20m and
422 100m isobaths. Station positions are indicated by the black dots on the 2 September image.

423
424 stations had concentrations $>1.0 \text{ mg m}^{-3}$, while at 29 stations they were 0.5 mg m^{-3} or less. The
425 highest surface concentration (1.7 mg m^{-3}) was found inshore just south of Galveston Bay.
426 Midwater maxima only exceeded 2 mg m^{-3} below 40m depth at offshore stations 27 and 28. This
427 is similar to summer conditions reported by Nowlin et al. (1998) and to previous data we have
428 collected during summer cruises in the northern Gulf of Mexico. Three days later, however,
429 when the inshore stations were reoccupied, mean fluorescence values showed $1-2 \text{ mg m}^{-3}$ at all
430 inshore stations, with concentrations up to 4.8 mg m^{-3} immediately offshore of Galveston in the
431 plume.

432

433 Satellite data, in contrast, showed considerably higher pigment values (Fig. 7). During mid-
434 August, the highest concentrations and the maximum offshore extent of potential blooms were
435 found off central Louisiana, within the 20m isobath. The zone of pigmented water narrowed
436 significantly from Sabine Lake (93.83°W) to Port Aransas Bay (97°W). This distribution likely
437 resulted from the pre-storm advection of nutrients from the Atchafalaya and Mississippi Rivers
438 coupled with generally low summer flows from Texas rivers. By 2 September, the highest
439 concentrations were detectable along the Texas coast from Sabine Lake to Corpus Christi Bay.
440 The widest zone of pigmented water extended well beyond the 20 m isobath east, southeast, and
441 south of Galveston Bay. Maximum satellite-derived coastal chlorophyll-*a* values near Galveston
442 Bay were 16 mg m⁻³, decreasing offshore to 10 mg m⁻³ at the 20 m isobath, and below 1 mg m⁻³
443 on the 100 m isobath (Fig. 8). During September, the zone of pigmented water on the shelf near
444 Galveston initially retreated shoreward, but moved offshore and southward later, with several
445 lobes reaching the 100 m isobath, although concentrations were only about one tenth of those
446 seen immediately after the storm.

447

448 4 Discussion

449

450 Previous studies of the impacts of hurricanes on the coastal zone suggest that the extreme rainfall
451 associated with such storms often leads to flushing of nutrients into the coastal bays and the
452 offshore coastal zone, as found in Biscayne Bay, Florida, following Hurricane Katrina in 2005
453 (Zhang et al., 2009), in the Neuse River/Pamlico Sound system in North Carolina (Paerl et al.,
454 2001, 2018; Peierls et al., 2003), in Chesapeake Bay (Roman et al., 2005), and in the Caribbean
455 in 1998 following Hurricane Georges (Gilbes et al., 2001). In all these cases, short-lived
456 phytoplankton blooms (2-3 weeks) resulted. It is also possible for offshore waters containing low
457 oxygen concentrations and raised nutrient concentrations to be injected onto the shelf from
458 offshore through upwelling. Chen et al. (2003), for example, while agreeing with Shiah et al.
459 (2000) that terrestrial runoff was a factor in increased local coastal productivity following such
460 storms in the East China Sea, suggested that the upwelling of subsurface Kuroshio water, thought
461 to result from “a larger buoyancy effect caused by the rains as well as the shoreward movement
462 of the Kuroshio caused by the typhoons,” was equally important, and that the “cross-shelf

463 upwelling of nutrient-rich Kuroshio water after the passage of typhoon Herb in a normally
464 “downwelling region” could even induce local hypoxia.

465

466 A third potential impact is local acidification resulting from the excessive rainfall in the coastal
467 region, as reported by Manzello et al. (2013) and Gray et al. (2012). Hicks et al. (2022) showed
468 that this occurred in Galveston Bay following Harvey, with the acidification lasting for three
469 weeks and causing undersaturation of calcium carbonate that may have affected the recovery of
470 local oyster reefs.

471

472 *Oxygen and nutrient variability*

473 Our data show very little sign of increased nutrient concentrations offshore, other than excess
474 phosphate seen during the first September cruise. Since Texas bays are oligotrophic during the
475 summer, the influx of freshwater resulted in higher concentrations of nutrients, particularly
476 nitrate and silicate, as well as blooms of phytoplankton and cyanobacteria within the bays (Liu et
477 al., 2019; Steichen et al., 2020). DIN concentrations, in particular, were greatly reduced two
478 weeks after the hurricane had passed through the region and were back to normal conditions by
479 November (Steichen et al., 2020, Fig. 8; J. Fitzsimmons, pers. comm.), with concentrations
480 above 5 $\mu\text{mol/L}$ only found in the uppermost parts of the system after about 15 September.
481 Silicate concentrations similarly dropped quickly within the first two weeks, although they
482 remained above 40 $\mu\text{mol/L}$ throughout Galveston Bay during the sampling period.

483

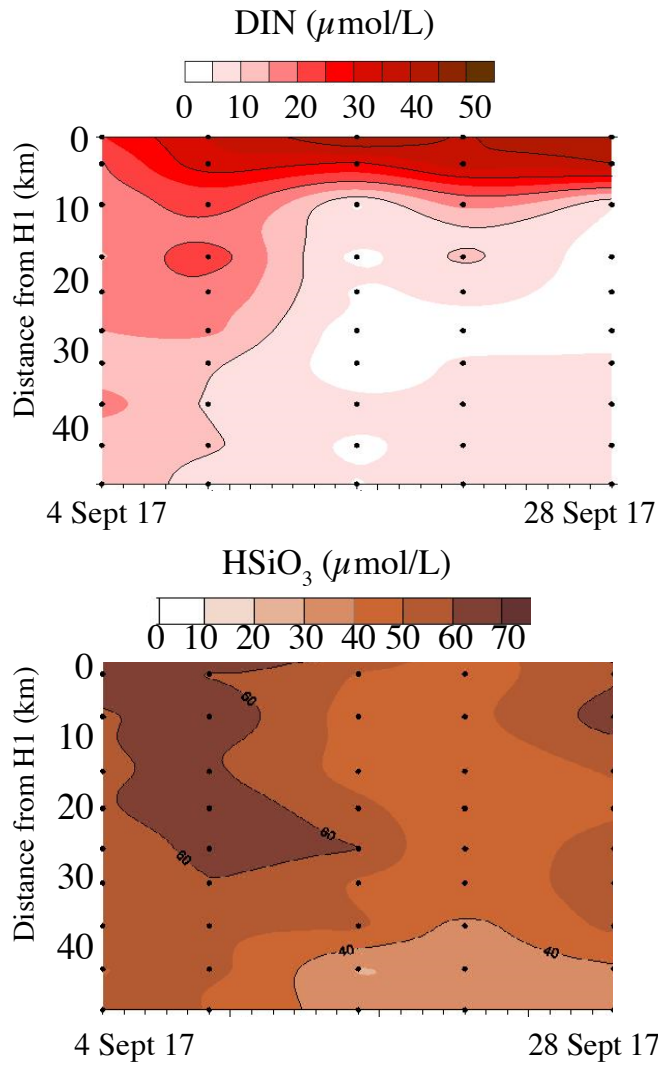
484 Following hurricane Harvey, low-oxygen water containing <160 $\mu\text{mol/L}$ and nitrate
485 concentrations of > 2 $\mu\text{mol/L}$ penetrated further onto the shelf during September than during
486 either August or November (Figs. 5, S3). The high salinity of this water mass (>36, Fig. 5)
487 suggests that it was Subtropical Underwater, which is found above 250 m in the northern Gulf
488 with typical core salinity of about 36.4 -36.5 near 100m depth in this region, and oxygen and
489 nitrate concentrations of about 110-150 $\mu\text{mol/L}$ and 6-15 $\mu\text{mol/L}$ respectively (Nowlin et al.,
490 1998). However, given the strong pycnocline shown by the salinity section (Fig. 5), there was
491 little opportunity for these additional nutrients to reach the surface layer and affect
492 phytoplankton production, and there is no evidence that such upwelling has resulted in hypoxia
493 in the past in this region.

494

495 Further south, the Matagorda-San Antonio-Aransas-Corpus Christi Bay system also showed
496 rapid short-term nutrient increases, followed in this case by hypoxia (Montagna et al., 2017;
497 Walker et al., 2021), but nutrient concentrations here were back to pre-storm concentrations by
498 early October (Walker et al., 2021). The levels in Guadeloupe Bay, an offshoot of San Antonio
499 Bay, were followed at fortnightly intervals from mid-August to mid-October and showed a rapid
500 increase in nitrate but slower increases in phosphate and silicate. This is not unexpected, given
501 that nitrate does not bind readily to sediment particles or organo-iron complexes like phosphate
502 and silicate (Lewin, 1961; Suess, 1981). Thus, it appears that the increases in nutrient
503 concentrations affected mainly the coastal bays and estuaries rather than the offshore coastal
504 zone. This backs up conclusions of Sahl et al. (1993) following a cruise along the Louisiana-
505 Texas shelf in March 1989 when river discharges were at their highest levels during that year.
506 They found that nutrients derived from bay systems dissipated within about 20km of the bay
507 mouths, and that higher nutrient concentrations below 80 m depth resulted from upwelling along
508 the shelf edge, in agreement with the work of Chen et al. (2003) and Walker et al. (2005).

509

510 Although nutrient fluxes were undoubtedly greatly increased immediately following the
511 hurricane, nutrient concentrations in Texas rivers are only sampled infrequently, and data do not
512 exist to allow us to calculate the overall fluxes during this period. However, the available data
513 suggest that absolute concentrations did not change very much following the hurricane in most
514 instances (Table 3). Coupled with the rapid decrease in river flow by about **7 September** (Fig.
515 S1), this suggests that excess nutrients in the bays and the coastal ocean were likely either taken
516 up by phytoplankton (within the bays) or diluted (offshore) by the time of our survey in late
517 September. Du et al. (2019) point out that while the salinity at the mouth of Galveston Bay was
518 back to normal about two weeks after the storm, it took almost two months to recover at stations
519 further inside the bay and the same time period at offshore buoys. Similar effects are likely at
520 other bay sites along the Texas coast.



521

522 **Fig. 8.** Surface nitrate plus nitrite (a) and silicate (b) concentrations ($\mu\text{mol/L}$) measured along a transect through
 523 Galveston Bay along the Houston Ship Channel. Sampling dates were 4 September, 9 September, 16 September, 21
 524 September, and 28 September 2017. Station H1 (0 km) was the innermost station in the bay, H10 was just outside
 525 the breakwater in the Gulf (see Steichen et al., 2020 for details).

Commented [PC6]: Concentrations corrected to $\mu\text{mol/L}$

526 Table 3. Nutrient concentrations in Texas rivers around the time of the hurricane ($\mu\text{mol/L}$). Data taken from USGS
527 and the Texas Commission on Environmental Quality (TCEQ) Clean Rivers Program for individual river basins.

528
529 a. Trinity River (Baytown; USGS site 08067525)

530 Date	531 Nitrate	532 Phosphate	533 Silicate
7.06.17	10.15	2.03	74.2
7.19.17	11.28	2.52	90.0
8.15.17	11.43	3.16	155.5
9.05.19	10.64	1.74	96.0
11.08.17	5.43	1.58	143.5

534
535
536
537 b. Trinity River (Liberty, USGS site 08067000)

8.16.17	<2.86	2.38	137.5
8.31.16	8.71	1.32	97.8
9.05.16	15.85	2.26	127.0

538
539
540
541 c. Brazos River (US 290; TCEQ site 11850)

7.26.17	41.40	<1.29
8.22.17	7.86	<1.29
9.27.17	12.86	2.26
10.25.17	37.86	2.90

542
543
544
545
546 d. Colorado River (La Grange; TCEQ site 12292)

6.06.17	2.86	92.58
8.08.17	2.86	118.06
10.02.17	2.14	86.45

547
548 e. San Antonio River (Goliad; TCEQ site 12791)

7.19.17	<3.57
9.06.17	<3.57
11.01.17	<3.57

558 *Salinity variability in the coastal zone*

559 Salinity changes were recorded at offshore moorings during and following the storms. During the
560 passage of the hurricane, the TABS moorings showed rapid decreases in salinity with a slow
561 increase thereafter (data not shown). Buoy X (offshore) showed the least variability, with
562 salinities remaining near 36.4 until **4 September 2017**, dropping briefly to 35.3, but recovering to
563 above 36 again by **6 September**. Buoy D, inshore near Corpus Christi, also recorded salinities of
564 about 36.6 until **23 August**, dropping to 34.7 on **26 August**, but were >36 a day later. Salinities
565 dropped again on **29 August**, remaining in the range 32-34 until **6 September**, after which they
566 dropped again to below 30, where they remained until **24 October 2017**, with a minimum salinity

567 of 20.51 on **13 September**. Further up the coast buoys B and F both experienced decreased
568 salinities (buoy W did not record salinities during the passage of the hurricane). Before the
569 hurricane, salinities in this region were in the range 32.5-34.5, with the higher salinities offshore.
570 Following the passage of the storm, buoy F recorded a minimum salinity of 15.25 on **1**
571 **September** and salinities <20 until **6 September**. A salinity of 30 was only recorded again here on
572 **8 September**. The inshore buoy B recorded minimum salinities in the range 19-21 on **30 August**.
573 These remained <23 until **9 September**, and below 30 for the remainder of the month, after which
574 they increased again to around 32. The fact that the minimum salinity was recorded at the
575 offshore mooring is presumably related to the strength of the plume emanating from Galveston
576 Bay with enough momentum to overcome the Coriolis force that would tend to push it to the
577 southwest close to the coast (Du et al., 2019).

578

579 These data suggest a slow southward movement of low salinity water along the coast (see Figs.
580 4c, d) after the hurricane as the coastal current was re-established. The easterly winds during
581 almost the whole of September assisted this downcoast movement, as described by Cochrane and
582 Kelly (1986). Mixing during the infrequent northerly wind bursts caused salinities to increase
583 again, although even in November salinities below 30 were still seen between Galveston Bay and
584 Matagorda-Corpus Christi Bays (Fig. 4e).

585

586 **Chlorophyll variability**

587 Assuming that chlorophyll-*a* can be used as a proxy for phytoplankton productivity, along the
588 Texas shelf and slope, we can use the MODIS satellite data to show how the phytoplankton
589 biomass varied following the hurricane. The prevailing currents during the latter half of
590 September (Fig. 3), would have moved the pigment concentrations further south and offshore,
591 where they decreased. Since our first post-storm cruise occurred between 22-27 September, we
592 would have missed the maximum extent of any offshore nutrient maximum and its associated
593 bloom. Given the potential discrepancy between satellite-derived and in situ values from CDOM
594 interference in the satellite estimates, however, we believe the higher concentrations in early
595 September shown in **Fig. 7** result largely from the hurricane stirring up bottom sediments in the
596 shallow coastal zone, and there was no evidence for upwelled nutrients resulting in blooms at the
597 shelf edge, as reported off Louisiana following Hurricane Ivan in 2004 (Walker et al., 2005) or in

Commented [PC7]: Most of the content of this paragraph has been moved to new section 3.5

598 the East China Sea by Chen et al. (2003). The accumulation of highly pigmented water between
599 Galveston Bay and Calcasieu Lake (93.45°W) in the 2 September image likely resulted from
600 convergence of the downcoast Louisiana river waters (Quigg et al., 2011) with upcoast
601 hurricane-related discharges from Texas, as surface currents at TABS buoy B were offshore and
602 decreased from $\sim 75 \text{ cm/s}$ to 20 cm/s during the period from 30 August to 3 September (Fig. 3).

603

604 *Why was there no hypoxia following Harvey?*

605 Although September is normally the month when the passage of storm front causes seasonal
606 hypoxia (oxygen concentrations $< 62 \mu\text{mol/L}$) in the northern Gulf of Mexico to end, the strong
607 stratification resulting from the freshwater input might have been expected to reduce oxygen
608 concentrations below the pycnocline. Rabalais et al. (1999) state that hypoxia can in fact occur in
609 almost any month if conditions, particularly stratification, are right. Hypoxia in the northern
610 Gulf of Mexico has three requirements: a high supply of nutrients, especially nitrogen, from
611 rivers or other terrestrial runoff, stable stratification with a mid-water pycnocline, and relatively
612 low wind conditions (Bianchi et al., 2010; Rabalais et al., 2007; Wiseman et al., 1997). While the
613 most intense hypoxia occurs over the Louisiana shelf (Rabalais et al., 1999), dissolved oxygen
614 levels below $30 \mu\text{mol/L}$ have been detected during NOAA SEAMAP cruises as far west as
615 96°W , with occasional samples between $30\text{-}60 \mu\text{mol/L}$ identified near Corpus Christi (see
616 <https://www.ncei.noaa.gov/maps/gulf-data-atlas/atlas.htm>, accessed 16 July 2020), as well as
617 following local flood events (DiMarco et al., 2012; Kealoha et al., 2020), and bacteria from
618 terrestrial sources have been found in sponges at the Flower Gardens Banks National Marine
619 Sanctuary near 28°N , 29.5°W (Shore et al., 2021).

620

621 While Texas hypoxia is typically linked to southwestward advection from the Mississippi and
622 Atchafalaya Rivers, high flow rates from local rivers have also been implicated (Harper et al.,
623 1981; Pokryfki and Randall, 1987; DiMarco et al., 2012). During the passage of Hurricane
624 Harvey, the torrential rainfall led to runoff that created a stable pycnocline, and calm conditions
625 after the storm meant that phytoplankton growth was possible. On the Louisiana shelf,
626 stratification is re-established within a few days of the passage of storm fronts or hurricanes and
627 bottom water oxygen depletion can begin rapidly once the storm has passed (e.g., Bianchi et al.,
628 2010; Jarvis et al., 2021). However, despite the strong stratification after Harvey, we found no

629 obvious signs of hypoxia over the Texas shelf, nor any increased nutrient concentrations, other
630 than phosphate, in coastal water. Plotting the difference in salinity between surface and bottom
631 samples, a measure of water column stability (DiMarco et al., 2012), against bottom oxygen
632 concentrations during the September cruise gave only a low correlation, with $R^2 = 0.15$ ($n = 38$),
633 as opposed to the 0.79 ($n = 14$) reported in 2007 by DiMarco et al. (2012). This suggests that
634 stratification by itself was not responsible for the observed bottom oxygen concentrations over
635 the shelf following Harvey.

636

637 The lack of hypoxia following Hurricane Harvey can therefore perhaps be explained by four
638 factors. First, only a limited flux of nutrients made it out of the bays and into the coastal zone,
639 where it was likely taken up rapidly by phytoplankton in the oligotrophic coastal waters, as seen
640 elsewhere. Additionally, southward and offshore advection of low salinity runoff increased the
641 rate of dilution through mixing with pre-existing low-nutrient surface shelf water. The largest
642 bay systems have relatively narrow entrances, which reduce the rate at which the fresh water can
643 escape – the main entrance to Galveston Bay, which includes the deep, dredged Houston Ship
644 Channel, is only 2.3 km wide and the turnover time for water is 15-60 days under normal
645 conditions, with shorter periods coinciding with flood conditions (Solis and Powell, 1999;
646 Rayson et al., 2016). Thyng et al. (2020) have estimated that the flushing of Galveston Bay
647 during Hurricane Harvey took only 2-3 days following the initial heavy rainfall. For the Corpus
648 Christi Bay/Aransas Bay system the turnover time under normal conditions is estimated to be
649 more than 300 days (Solis and Powell, 1999), similar to Pamlico Sound (Paerl et al., 2001).

650

651 Second, the sheer volume of water rapidly removed available soluble nutrients within the first
652 few hours so that runoff later during the storm was essentially pure rainwater. It is known that
653 large percentages of available nutrients are removed in stormwater runoff in the first minutes or
654 hours following a downpour and concentrations then drop (e.g., Cordery, 1977; Horner et al.,
655 1994; Fellman et al., 2008). Similar effects have been reported for trace metals in the floodplain
656 of the Pearl River in Mississippi (Shim et al., 2017), where maximum downstream
657 concentrations were not found following peak flows. These authors suggested that the rapid
658 flushing overwhelmed the rate at which soluble metal-organic complexes could be regenerated.
659 As the hurricane occurred in late summer, any nutrients applied to cropland along the Texas

660 coastline in spring would largely have been taken up by the vegetation and so be unavailable for
661 washout. While Corpus Christi (population ~325,000) and Houston (~4 million) are large
662 population centers with multiple sewage treatment plants that flooded following the hurricane,
663 both are sited upstream of large bay systems that would have attenuated the speed at which
664 stormwater runoff dissipated. The rate of change of nutrient concentrations in Galveston Bay
665 (Fig. 8) shows that uptake within the bay system was likely considerably more important than
666 flushing, even with the apparently short flushing time calculated by Thyng et al (2020).

667

668 While nutrient flushing was reduced following the hurricane, the same is unlikely to be true for
669 sediment. As shown in Fig. S2, and as discussed by D'Sa et al. (2018), Du et al. (2019), and
670 Steichen et al. (2020), large sediment plumes occurred off the mouths of major bays and rivers.
671 The heavy sediment loads would have both increased the turbidity of the water column and
672 thereby reduced light intensity in the euphotic zone, and led to reduced phosphate concentrations
673 as phosphate is known to bind to sediment particles (e.g., Suess, 1981). Both factors would have
674 contributed to reduced phytoplankton production, a major factor in hypoxia formation (Bianchi
675 et al., 2010). While phosphate concentrations in the coastal zone were highest during the first
676 September cruise, suggesting at least some terrestrial runoff immediately following the hurricane
677 and possibly desorption from suspended sediment, the low nitrate concentrations seen during this
678 cruise and the low chlorophyll fluorescence suggests only a short-term phytoplankton bloom at
679 most, again similar to previous observations (e.g., Roman et al., 2005).

680

681 The final potential control is sediment composition along the Texas shelf. Most sediments in this
682 region are coarse, sandy, and contain little organic matter (Hedges and Parker, 1974). This is in
683 contrast to the Louisiana shelf, where muddy, organic sediments are quite common and act as a
684 reservoir of material that can continue to reduce oxygen concentrations once stratification is
685 established (Bianchi et al., 2010; Corbett et al., 2006; Eldridge and Morse, 2008; Turner et al.,
686 2008). This is especially true within coastal embayments, such as Terrebonne Bay, LA, where
687 the organic carbon content can exceed 5% thanks to organic matter input from the surrounding
688 marshes and swamps (Hedges and Parker, 1974; Bianchi et al., 2009, 2010). Even near the
689 Mississippi and Atchafalaya Rivers, however, typical organic carbon sediment content on the
690 shelf is generally <2% (Gordon and Goni, 2004; Gearing et al, 1977), while further west off the

691 Texas coast it is typically < 1% (Hedges and Parker, 1974, Bianchi et al., 1997). This suggests
692 that organic matter along the Texas shelf is refractory, and less likely to add to any oxygen
693 demand, and that hypoxia on the Texas shelf is generally driven by water column respiration as
694 discussed by Hetland and DiMarco (2008). In this region stratification alone is not sufficient to
695 bring about hypoxic conditions in the absence of high nutrient concentrations and phytoplankton
696 blooms.

697

698 **5 Conclusions**

699 Although Hurricane Harvey led to pronounced flooding and exceptional freshwater runoff along
700 the Texas coast, it did not lead to lasting high nutrient concentrations offshore, largely because of
701 dilution by the rainfall, the likely rapid uptake by phytoplankton of nutrients within the bays, and
702 mixing with oligotrophic coastal water. While the most pronounced changes in nutrient
703 concentrations were seen in the coastal bays, changes from background levels were short-lived,
704 and conditions were essentially back to normal by November, some eight weeks after the
705 hurricane, following northerly wind bursts that caused mixing within the water column. There
706 was also no evidence of low oxygen water upwelled by the hurricane reaching the inner shelf
707 from offshore, as suggested following hurricanes elsewhere. While an apparent transient bloom
708 of phytoplankton was observed in satellite imagery offshore following the hurricane, its short
709 existence and the potential for contamination of satellite estimates by CDOM suggests that
710 hypoxia could not develop despite the stratification because nutrient concentrations were too low
711 to support continued phytoplankton productivity. Similarly, the lack of an organic matter
712 reservoir in the shelf sediments means there is no additional oxygen demand in Texas bottom
713 waters, and hypoxia here depends on water column decomposition.

714

715 **6 Acknowledgements**

716 We are grateful to the Captains and crews of the R.V. *Manta* and R.V. *Point Sur* for their
717 excellent service during the cruises, and to the enthusiasm of the students and technicians who
718 helped with data collection. The TABS system is funded by the Texas General Land Office and
719 operated by the TAMU Geochemical and Environmental Research Group. Cruises were funded
720 by the Texas Governor's Fund through the Texas OneGulf Center of Excellence and an NSF
721 RAPID award (OCE-1760381) to Drs. Knap, Chapman and DiMarco. A.H. K. would also like to

722 acknowledge financial support from the G. Unger Vetlesen Foundation. We thank Ysabel Wang
723 and Jamie Steichen for help with the figures, and Alaric Haag for assistance with SeaDAS image
724 processing. Walker and Haag thank the Gulf of Mexico Coastal Ocean Observing System
725 (GCOOS) for funding LSU Earth Scan Laboratory activities. Bathymetry shown in satellite
726 imagery was provided by GEBCO Compilation Group (2020) GEBCO 2020 Grid
727 (doi:10.5285/a29c5465-b138-234d-e053-6c86abc040b9). Funding sources had no involvement
728 in study design, data collection and interpretation, or manuscript preparation.

729

730 Data have been submitted to the Biological and Chemical Oceanography Data Management
731 Office (BCO-DMO). The titles and DOIs are: Processed CTD profile data from all electronic
732 sensors mounted on rosette from R/V Pt. Sur PS 18-09 Legs 01 and 03, Hurricane Harvey
733 RAPID Response cruise (western Gulf of Mexico) September-October 2017
734 (DOI:10.26008/1912/bco-dmo.809428.1); Hydrographic, nutrient and oxygen data from CTD
735 bottles and beam transmission and fluorescence data from CTD profiles during R/V Point Sur
736 PS1809 (HRR legs 1, 2, 3) at the Gulf Mexico, Louisiana and Texas coast, Sept-Oct 2017
737 (doi:10.1575/1912/bco-dmo.784290.1).

738

739 **7 Credit author statement**

740 The project was conceptualized by SFD and AHK; PC and SFD conducted investigations on all
741 cruises and collected and analyzed the initial data; AQ provided data from Galveston Bay; NDW
742 provided satellite imagery. PC wrote the initial draft; all authors provided comments and edits.
743 The authors declare that they have no conflict of interest.

744

745 **References**

746 Ahn, J.H., Grant, S.B., Surbeck, C.Q., DiGiacomo, P.M., Nexlin, N., Jiang, S.: Coastal Water
747 Quality Impact of Stormwater Runoff from an Urban Watershed in Southern California.
748 *Environ. Sci. Technol.*, 39, 5940-5963, doi:10.1021/es0501464, 2005

749 Balaguru, K., Foltz, G.R., Leung, L.R.: Increasing magnitude of hurricane rapid intensification in
750 the central and eastern tropical Atlantic. *Geophys. Res. Lett.*, 45, 4238–4247, doi:
751 10.1029/2018GL077597, 2018

752 Bianchi, T.S., DiMarco, S.F., Smith, R.W., Schreiner, K.M.: A gradient of dissolved organic
753 carbon and lignin from Terrebonne-Timbalier Bay estuary to the Louisiana shelf (USA).
754 *Mar. Chem.*, 117, 32-41, doi: 10.1016/j.marchem.2009.07.010, 2009.

755 Bianchi, T.S., DiMarco, S.F., Cowan, J.H., Hetland, R.D., Chapman, P., Day, J.W.,
756 Allison, M.A.: The Science of Hypoxia in the Northern Gulf of Mexico: A Review.
757 *Sci. Total Environ.*, 408, 1471-1484; doi: 10.1016/j.scitotenv.2009.11.047, 2010.

758 Bianchi, T.S., Lambert, C.D., Santschi, P.H., Guo, L.: Sources and transport of land-derived
759 particulate and dissolved organic matter in the Gulf of Mexico (Texas slope/shelf): The use
760 of lignin-phenols and loliolides as biomarkers. *Org. Geochem.*, 27, 65-78, doi:
761 10.1016/S0146-6380(97)00040-5, 1997.

762 Blake, E.S., Zelinsky, D.A.: *Hurricane Harvey*. NOAA National Hurricane Center Tropical
763 Cyclone Report AL092017, 2018.

764 Chen, C-T. A., Liu, C-T., Chuang, W.S., Yang, Y.J., Shiah, F-K., Tang, T.Y., Chung, S.W.:
765 Enhanced buoyancy and hence upwelling of subsurface Kuroshio waters after a typhoon in
766 the southern East China Sea. *J. Mar. Sys.*, 42, 65-79, doi :10.1016/S0924-7963(03)00065-4,
767 2003.

768 Cochrane, J.D., Kelly F.J.: Low-frequency circulation on the Texas-Louisiana continental shelf.
769 *J. Geophys. Res.* 91, 10645-10659, doi: 10.1029/JC091iC09p10645, 1986.

770 Corbett, D.R., McKee, R.A., Allison, M.A.: Nature of decadal-scale sediment accumulation in
771 the Mississippi River deltaic region. *Cont. Shelf Res.*, 26, 2125-2140, doi:
772 10.1016/j.csr.2006.07.012, 2006.

773 Cordery, I.: Quality characteristics of urban storm water in Sydney, Australia. *Water Resources
774 Res.*, 13, 197-202, doi: 10.1029/WR013i001p00197, 1977.

775 De Carlo, E., Hoover, D.J., Young, C.W., Hoover, R.S., Mackenzie, F.T.: Impact of storm runoff
776 from tropical watersheds on coastal water quality and productivity. *Appl. Geochem.*, 22,
777 1777-1797. doi: 10.1016/j.apgeochem.2007.03.034, 2007.

778 DiMarco, S.F., Strauss, J., May, N., Mullins-Perry, R.L., Grossman, E. Shormann, D.: Texas
779 coastal hypoxia linked to Brazos River discharge as revealed by oxygen isotopes. *Aq.*
780 *Geochem.*, 18, 159-181, doi:10.1007/s10498-011-9156-x, 2012.

781 DiMarco, S.F., Zimmerle, H.M. 2017. *MCH Atlas: Oceanographic Observations of the*
782 *Mechanisms Controlling Hypoxia Project*. Texas A&M University, Texas Sea Grant
783 Publication TAMU-SG-17-601, 300 pp. (available online at <http://mchatlas.tamu.edu>).

784 D'Sa, E., Joshi, I., Liu, B.: Galveston Bay and coastal ocean optical-geochemical response to
785 Hurricane Harvey from VIIRS ocean color. *Geophys. Res. Lett.*, 45, 10,579-10,589
786 doi:10.1029/2018GL079954 2018.

787 Du, J., Park, K., Dellapenna, T.M., Clay, J.C.: Dramatic hydrodynamic and sedimentary
788 responses in Galveston Bay and adjacent inner shelf to Hurricane Harvey. *Sci. Total.*
789 *Environ.*, 653, 554-564, doi: 10.1016/j.scitotenv.2018.10.403, 2019.

790 Eldridge, P.M., Morse, J.W.: Origins and temporal scales of hypoxia on the Louisiana shelf:
791 importance of benthic and sub-pycnocline water column metabolism. *Mar. Chem.*, 108, 159-
792 171, doi: 10.1016/j.marchem.2007.11.009, 2008.

793 Emanuel, K.: Assessing the present and future probability of Hurricane Harvey's
794 rainfall. *Proc. Natl. Acad. Sci. U.S.A.*, 114, 12681-12684, doi:10.1073/
795 pnas.1716222114, 2017.

796 Fellman, J.B., Hood, E., Edwards, R.T., D'Amore, D.V.: Return of salmon-derived nutrients
797 from the riparian zone to the stream during a storm in southeastern Alaska. *Ecosystems*, 11,
798 537-544, doi: 10.1007/s10021-008-9139-y, 2008.

799 Fritz, A., Samenow, J. 2017. Harvey Unloaded 33 Trillion Gallons of Water in the U.S. The
800 Washington Post, September 2, 2017. <https://www.washingtonpost.com/news/capital-weather-gang/wp/2017/08/30/harvey-has-unloaded-24-5-trillion-gallons-of-water-on-texas-and-louisiana/>.

803 Gearing, P., Plucker, F.T., Parker, P.L.: Organic carbon stable isotope ratios of continental
804 margin sediments. *Mar. Chem.*, 5, 251-266, doi: 10.1016/0304-4203(77)90020-2, 1977.

805 Gilbes, F., Armstrong, R.A., Webb, R.M.T., Muller-Karger, F.E.: SeaWiFS helps assess
806 hurricane impact on phytoplankton in Caribbean Sea. *Eos, Trans. Amer. Geophys. Union*, 82,
807 529, 533, doi: 10.1029/01EO00314, 2001.

808 Gordon, E.S., Goni, M.A.: Controls on the distribution and accumulation of terrigenous organic
809 matter in sediments from the Mississippi and Atchafalaya river margin. *Mar. Chem.*, 92, 331-
810 352, doi: 10.1016/j.marchem.2004.06.035, 2004.

811 Gray, S.E.C., DeGrandpre, M.D., Langsdon, C., Corredor, J.E. Short-term and seasonal pH,
812 pCO₂ and saturation state variability in a coral reef ecosystem. *Glob. Biogeochem. Cycles*
813 26, GB3012, 2012.

814 Harper, D.E. Jr., Salzer R.R., Case R.J.: The occurrence of hypoxic bottom water off the upper
815 Texas coast and its effect on the benthic biota. *Contr. Mar. Sci.*, 24, 53-79, 1981.

816 Hedges, J.I. , Parker, P.L.: Land-derived organic matter in surface sediments from the Gulf of
817 Mexico. *Geochim. Cosmochim. Acta*, 40, 1019-1029, doi: 10.1016/0016-7037(76)90044-2,
818 1974.

819 Hetland, R.D., DiMarco, S.F.: How does the character of oxygen demand control the structure of
820 hypoxia on the Texas-Louisiana continental shelf? *J. Mar. Sys.*, 70, 49-62, doi:
821 10.1016/j.jmarsys.2007.03.002, 2008.

822 Hicks, T.L., Shamberger, K.E.F., Fitzsimmons, J.N., Jensen, C.C., DiMarco, S.F. Tropical
823 cyclone-induced coastal acidification in Galveston Bay, Texas. *Commun. Earth Environ.* 3,
824 297, doi:10.1038/s43247-022-00608-1, 2022.

825 Horner, R. R., Skupien, J. J., Livingston, E. H., and Shaver, H. E.: *Fundamentals of urban runoff
826 management: Technical and institutional issues*. Terrene Institute, Washington, D.C., 1994.

827 Jarvis, B.M., Greene, R.M., Wan, Y., Lehrter, J.C., Lowe, L.L., Ko, D.S: Contiguous low
828 oxygen waters between the continental shelf hypoxia zone and nearshore coastal waters of
829 Louisiana, USA: interpreting 30 years of profiling data and three-dimensional ecosystem
830 modeling. *Environ. Sci. Technol.*, 55, 4709-4719, doi: 10.1021/acs.est.0c05973, 2021.

831 Kealoha, A.K., Doyle, S.M., Shamberger, K.E.F., Sylvan, J.B., Hetland, R.D., DiMarco, S.F.:
832 Localized hypoxia may have caused coral reef mortality at the Flower Garden Banks. *Coral
833 Reefs*, 39, 119-132, doi: 10.1007/s00338-019-01883-9, 2020.

834 Lewin, J.C. : The dissolution of silica from diatom walls. *Geochem. Cosmochim. Acta* 21, 182-
835 198.

836 Liu, B., D'Sa, E., Joashi, I.: Floodwater impact on Galveston Bay phytoplankton taxonomy,
837 pigment composition and photo-physiological state following Hurricane Harvey from field
838 and ocean color (Sentinel-3A OLCI) observations. *Biogeosciences*, 16, 1975-2001;
839 doi:10.5194/bg-2018-504, 2019.

840 Mallin, M.A., Corbett, C.A.: How hurricane attributes determine the extent of environmental
841 effects: multiple hurricanes and different coastal systems. *Estuar. Coasts.*, 29, 1046-1061,
842 doi: 10.1007/BF02798667, 2006.

843 Manzello, D., Enochs, I., Musielewicz, S., Carlton, R., Gledhill, D. Tropical cyclones cause
844 CaCO₃ undersaturation of coral reef seawater in a high-CO₂ world. *J. Geophys. Res. Oceans*
845 118, 5312-5321, 2013.

846 Montagna, P., Hu, X., Walker, L., Wetz, M. 2017. Biogeochemical impact of Hurricane Harvey
847 on Texas coastal lagoons. AGU Fall Meeting Abstract #NH23E-2797.

848 Nowlin, W.D.Jr., Jochens, A.E., Reid, R.O., DiMarco, S.F. 1998. Texas-Louisiana Shelf
849 Circulation and Transport Processes Study: Synthesis Report. *PCS Study MMS 98-0035*. U.S.
850 Department of the Interior, Minerals Management Service, Gulf of Mexico OCS Region,
851 New Orleans, LA.

852 Paerl, H.W., Bales, J.D., Ausley, L.W., Buzzelli, C.P., Crowder, L.B., Eby, L.A., Fear, J.M., Go,
853 M., Peierls, B.L., Richardson, T.L., Ramus, J.S.: Ecosystem impacts of three sequential
854 hurricanes (Dennis, Floyd, and Irene) on the United States' largest lagoonal estuary,
855 Pamlico Sound, NC. *Proc. Natl. Acad. Sci. U.S.A.*, 98, 5655-5660, doi:
856 10.1073/pnas.101097398, 2001.

857 Paerl, H.W., Crosswell, J.R., Van Dam, B., Hall, N.S., Rossignol, K.L., Osburn, C.L., Hounshell,
858 A.G., Sloup, R.S., Harding, L.W. Jr.: Two decades of tropical cyclone impacts on North
859 Carolina's estuarine carbon, nutrient and phytoplankton dynamics: implications for
860 biogeochemical cycling and water quality in a stormier world. *Biogeochemistry*, doi:
861 10.1007/s10533-018-0438-x, 2018.

862 Paerl, H.W., Valdes, L.M., Joyner, A.R., Peierls, B.L., Piehler, M.F., Riggs, S.R., Christian,
863 R.R., Eby, L.A., Crowder, L.B., Ramus, J.S., Clesceri, E.J., Buzzelli, C.P., Luettich, R.A.:
864 Ecological response to hurricane events in the Pamlico Sound system, North Carolina, and
865 implications for assessment and management in a regime of increased frequency. *Estuar.
Coasts*, 29, 1033-1045, doi:10.1007/BF02798666, 2006.

867 Peierls, B.L., Christian, R.R., Paerl, H.W.: Water quality and phytoplankton as indicators of
868 hurricane impacts on a large estuarine system. *Estuaries*, 26, 1329-1343, doi:
869 10.1007/BF02803635, 2003.

870 Pokryfki, L., Randall, R.E.: Nearshore hypoxia in the bottom water of the northwestern Gulf of
871 Mexico from 1981 to 1984. *Mar. Environ. Res.*, 22, 75-90, doi: 10.1016/0141-
872 1136(87)90081-X, 1987.

873 Potter, H., DiMarco, S.F., Knap, A.H.: Tropical cyclone heat potential and the rapid
874 intensification of hurricane Harvey in the Texas Bight. *J. Geophys. Res. (Oceans)*, 124,
875 2440-2451, doi:10.1029/2018JC014776, 2019.

876 Quigg, A., Sylvan, S.B., Gustafson, A.B., Fisher, T.R., Oliver, R.L., Tozzi, S., Ammerman, J.W.:
877 Going West: nutrient limitation of primary production in the northern Gulf of Mexico and the
878 importance of the Atchafalaya River. *Aq. Geochem.*, 17, 519-544, doi: 10.1007/s10498-011-
879 9134-3, 2011.

880 Rabalais, N.N., Turner, R.E., Justic, D., Dortch, Q., Wiseman, W.J., Jr.: Characterization of
881 Hypoxia: Topic 1 Report for the Integrated Assessment of Hypoxia in the Gulf of Mexico.
882 NOAA Coastal Ocean Program Decision Analysis Series No. 15. NOAA Coastal Ocean
883 Program, Silver Spring, Maryland, 1999.

884 Rabalais, N.N., Turner, R.E., Sen Gupta, B.K. , Boesch, D.F. , Chapman, P., Murrell, M.C.:
885 Hypoxia in the northern Gulf of Mexico: Does the science support the plan to reduce,
886 mitigate and control hypoxia? *Estuar. Coasts*, 30, 753-772, doi: 10.1007/BF02841332, 2007.

887 Rayson, M.D., Gross, E.S., Hetland, R.D., Fringer, O.B.: Time scales in Galveston Bay: an
888 unsteady estuary. *J. Geophys. Res. (Oceans)*, 121, 2268-285, doi: 10.1002/2015JC011181,
889 2016.

890 Roman, M.R., Adolf, J.E., Bichy, J., Boicourt, W.C., Harding, L.W., Houde, E.D., Jung, S.,
891 Kimmel, D.G., Miller, W.D., Zhang, X.: Chesapeake Bay plankton and fish abundance
892 enhanced by Hurricane Isabel. *EOS*, 86, 261-265, doi: 10.1029/2005EO280001, 2005.

893 Sahl, L.E., Merrell, W.J., Biggs, D.C.: The influence of advection on the spatial variability of
894 nutrient concentrations on the Texas-Louisiana continental shelf. *Cont. Shelf. Res.*, 13, 233-
895 251; doi: 10.1016/0278-4343(93)90108-A, 1993.

896 Shiah, F.K., Chang, S.W., Kao, S.J., Gong, G.C., Liu, K.K.: Biological and hydrographical
897 responses to tropical cyclones (typhoons) in the continental shelf of the Taiwan Strait. *Cont.*
898 *Shelf. Res.*, 20, 2029-2044, doi: 10.1016/S0278-4343(00)00055-8, 2000.

899 Shim, M.J., Cai, Y., Guo, L., Shiller, A.M.: Floodplain effects on the transport of dissolved and
900 colloidal trace elements in the East Pearl River, Mississippi. *Hydrol Proc.*, 31, 1086-1099,
901 doi: 10.1002/hyp.11093, 2017.

902 Shore, A., Sims, J.A., Grimes, M., Howe-Kerr, L.I., Grupstra, C.G.B., Doyle, S.M., Stadler, L.,
903 Sylvan J.B., Shamberger, K.E.F., Davies, S.W., Santiago-Vazquez, L.Z., Correa, A.N.S.: On
904 a reef far, far away: Anthropogenic impacts following extreme storms affect sponge health
905 and bacterial communities. *Front. Mar. Sci.*, 8: 608036, doi: 10.3389/mars.2021.608036,
906 2021.

907 Solis, G.S., Powell, G.L. : Hydrography, mixing characteristics, ands residence times of Gulf of
908 Mexico estuaries. In: Bianchi, T.S., Pennock, J.R., Twilley, R.R. (eds). *Biogeochemistry of*
909 *Gulf of Mexico Estuaries*, John Wiley, NY, pp. 29-61, 1999.

910 Steichen, J.L., Labonte, J.M., Windham, R., Hala, D., Kaiser, K., Setta, S., Faulkner, P.C.,
911 Bacosa, H., Yan, G., Kamalanathan, M., Quigg, A.: Microbial, physical and chemical
912 changes in Galveston Bay following an extreme flood event, Hurricane Harvey. *Front. Mar.*
913 *Sci.*, 7, 186, doi:10.3389/fmars.2020.00186, 2020.

914 Suess, E.: Phosphate regeneration from sediments of the Peru continental margin by dissolution
915 of fish debris. *Geochem. Cosmochim. Acta*, 45, 577-588, doi: 10.1016/0016-7037(81)90191-
916 5, 1981.

917 Sylvan, J.B., Dortch, Q., Nelson, D.M., Brown, A.F.M., Morrison, W., Ammerman, J.W.:
918 Phosphorus limits phytoplankton growth on the Louisiana shelf during the period of hypoxia
919 formation. *Environ. Sci. Tech.*, 40, 7548-7553, doi : 10.1021/es061417t, 2006.

920 Sylvan, J.B., Quigg, A., Tozzi, S., Ammerman, J.W. : Eutrophication induced phosphorus
921 limitation in the Mississippi River plume: evidence from fast repetition rate fluorometry.
922 *Limnol. Oceanogr.*, 52, 2679-2685, doi: 10.4319/lo.2007.52.6.2679, 2007.

923 Thyng, K.M., Hetland, R.D., Socolofsky, S.A., Fernando, N., Turner, E.L., Schoenbaechler, C.:
924 Hurricane Harvey caused unprecedeted freshwater inflow to Galveston Bay. *Estuar. Coasts*,
925 doi:10.1007/s12237-020-00800-6, 2020.

926 Trenberth K.E., Chang L., Jacobs P., Zhang Y., Fasullo, J.: Hurricane Harvey links to ocean heat
927 content and climate change adaptation. *Earth's Future* 6, 730-744, doi:
928 10.1029/2018EF000825, 2018.

929 Turner R.E., Rabalais N.N., Justic D.: Gulf of Mexico Hypoxia: Alternate States and a Legacy.
930 *Environ. Sci. Technol.*, 42, 2323–2327, doi:10.1021/es071617k, 2008.

931 Walker, L.M., Montagna, P.A., Hu, X., Wetz, M.S.: Timescales and magnitude of water quality
932 change in three Texas estuaries induced by passage of Hurricane Harvey. *Estuar. Coasts*, 44,
933 960-971, doi: 10.1007/s12237-020-00846-6, 2021.

934 Walker, N.D.: Wind and eddy-related shelf/slope circulation processes and coastal upwelling in
935 the Northwestern Gulf of Mexico. In: Sturges W, Lugo-Fernandez A, editors. *Circulation in*
936 *the Gulf of Mexico: Observations and Models*. *Geophys. Monographs* 161, American
937 *Geophysical Union*, 295-313, doi:10.1029/161GM21, 2005.

938 Walker, N.D., Leben, R.R., Balasubramanian, S.: Hurricane-forced upwelling and chlorophyll *a*
939 enhancement within cold-core cyclones in the Gulf of Mexico. *Geophys. Res. Lett.* 32,
940 doi:10.1029/2005GL023716, 2005.

941 WHPO. 1994. *WHP Operations and Methods*. WOCE Hydrographic Office Report 91/1, as
942 revised, WOCE Hydrographic Programme Office, Woods Hole, MA.

943 Wiseman, W.J., Rabalais, N.N., Turner, R.E., Dinnel, S.P., McNaughton, A.: Seasonal and
944 interannual variability within the Louisiana coastal current: stratification and hypoxia. *J.*
945 *Mar. Sys.*, 12, 237-248, doi: 10.1016/S0924-7963(96)00100-5, 1997.

946 Zhang, J.-Z., Kelbie, C.R., Fischer, C.J., Moore, L.: Hurricane Katrina induced nutrient runoff
947 from an agricultural area to coastal waters in Biscayne Bay, Florida. *Est. Coastal Shelf Sci.*,
948 84, 209-218, doi: 10.1016/j.ecss.2009.06.026, 2009.

949